Wireless Sensor Networks for Detection and Localization of Subsea Oil Leakages

Gianluca Tabella, *Graduate Student Member, IEEE*, Nicola Paltrinieri, Valerio Cozzani,
and Pierluigi Salvo Rossi, *Senior Member, IEEE*

***Abstract*—This work studies the impact of Wireless Sensor Networks (WSNs) for oil spill detection and localization in Subsea Production Systems. The case study is the Goliat FPSO, with a realistic assumption about the presence of a WSN built upon the existing passive acoustic sensors installed on each subsea template to monitor the manifold. The sensors take local binary decisions regarding the presence/absence of a spill by performing an energy test. A Fusion Center (FC) collects such local decisions and provides a more reliable global binary decision. The Counting Rule (CR) and a modified Chair-Varshney Rule (MCVR) are compared. An objective function based on the Receiver Operating Characteristic (ROC) is used for threshold design. The FC, in case of a spill detection, provides an estimated position of the leak source. Four localization algorithms are explored: *Maximum A-Posteriori* (MAP) estimation, *Minimum Mean Square Error* (MMSE) estimation, and two heuristic centroid-based algorithms. Detection and localization performances are assessed in comparison to the (position) Clairvoyant Chair-Varshney Rule (CVR) and to the Cramér-Rao Lower Bound (CRLB), respectively. The considered framework requires the prior knowledge of the involved subsea production system in terms of components that in case of failure would cause a leakage and their corresponding failure rates.**

***Index Terms*—Data fusion, leak detection, leak localization, oil spill, subsea production system, wireless sensor network.**
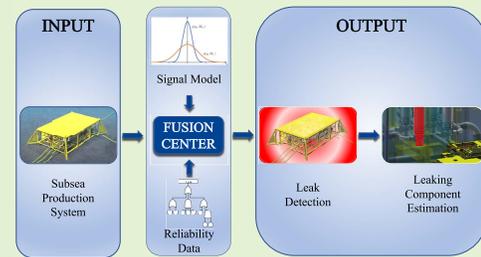
I. INTRODUCTION

THE Oil&Gas industry over the last few decades has developed new technologies for the exploitation of offshore resources previously technologically inaccessible or economically unfeasible. A relevant example is the use of Subsea Production Systems (SPS) connected to a close fixed platform, a floating system such as Floating Production Storage and Offloading (FPSO) Unit, Single Point Anchor Reservoir (SPAR) platform, Tension-Leg Platform (TLP), a Semi-submersible platform, or directly to the shore (less common option) [1].

SPSs are solutions that move part of the equipment on the seabed, in particular they transfer the *Christmas trees* (which are named *subsea trees* in this specific configuration in opposition to the *surface trees* present on traditional production platforms). A SPS allows a single platform to be equipped with several subsea trees. Usually the outlet streams of a group of neighboring subsea trees are connected to a *manifold* using pipes called *jumpers*. Manifolds are used to mix flows in a single stream before being transferred topside through *production risers* (some preliminary treatment like separation can be occasionally performed subsea). Sometimes multiple components of the SPS are gathered together in a single structure called *template*. The topside operators can control the SPS using *umbilicals*, which are bundles of flexible tubes and electrical conductors necessary for the transfer of the control fluid (necessary for the hydraulic control system), the transfer of chemicals (e.g. corrosion inhibitors, wax inhibitors, etc.), the powering of the subsea electrical components, and

the collection of the information coming from the sensors. A description of a SPS has been given by Bai Y. and Bai Q. [2].

This solution allows for oil extraction in deep waters, which is normally out of range for fixed platforms, and provides more effective field exploitation due to its versatility [3]. On the other hand, having a SPS means to have a greater number of components located on the seabed that can be subject to failure. In case a spill occurs, in fact, there is an increased difficulty to detect it as this will be happening in deep waters, which results in delayed production shutdowns with a consequent risk for workers' safety and the environment. Furthermore, having a spill originated on the seabed makes its localization more complex as a visual inspection is clearly not possible forcing costly inspections performed by Remotely Operated Vehicles (ROVs) [4]. Reducing the inspection time by having an estimated leak position can be vital to reduce the economic loss. For this reason, the presence of a Leak Detection System (LDS) capable to quickly detect and localize oil leakages is of paramount importance.

It is important to mention that the effectiveness of a LDS lies also in the quality of its integration into a risk management framework so that the increased level of knowledge on the SPS can be fully exploited. A proper integration can be obtained when the *Dynamic Risk Management Framework* (DRMF) is employed. The DRMF is a process open to external experience and early warnings allowing the integration of unknown information. Increased awareness of risks related to unknown events may lead to a learning and understanding phase (based on *monitoring* and *review* of accumulated information). *Horizon screening*, *hazard identification*, *assessment*, and final *decision/action* are the steps required by the DRMF to exhaustively evaluate the risks associated with known potential accident scenarios. Iterative updates are necessary to employ the DRMF as an adaptive process [5]–[8]. From this perspective, a LDS represents an early warning subsystem, part of a decision-support system related to actions such as plant shutdown and maintenance.

A. Related Work

Current technologies for leak detection rely on both internal methods based on measurements of process variables (e.g. flow rate and pressure) and external methods where sensors monitor the SPS's surrounding environment. Their characteristics have been extensively studied and most of these sensors are already in place in several offshore fields [9], [10] and their use is subject to strict quality standards [11]. A key feature of leakages is their associated acoustic signal that can be sensed via passive acoustic sensors [12], [13]. Unlike other technologies (e.g. capacitive sensors) that need to be in direct contact with the leaking fluid, passive acoustic sensors exhibit a much broader detection range. Also, their installation is easy and cost-effective as opposed to fiber optic cables. However, passive acoustic sensors are extremely sensitive to measurement noise with consequent difficulty in detecting smaller leaks [9]–[11]. The above-mentioned characteristics suggest the use of LDS based on acoustic sensors working as nodes of a WSN. Although the use of WSNs for leak detection purposes has been considered mainly in the monitoring of Oil&Gas

pipelines [14]–[16], some recent works have focused on the monitoring of a SPS through WSNs showing its benefits, especially from the point of view of the DRMF [17]–[19].

The field of data fusion in distributed WSN for event detection has its first big contribution from the initial work in [20]. Overtime, there has been a growing interest in distributed WSN where the sensors transmit binary decisions to a Fusion Center (FC) as this lowers communications and processing costs [21]. The following is a list of the main contributions for such kind of detection problem. In [22], [23] some fusion rules such as the Chair-Varshney Rule (CVR) and the Counting Rule (CR) have been proposed addressing also the problem of the detection performed locally by the sensors. In [24] a sub-optimal and a heuristic fusion rule, respectively called Maximum Ratio Combining Fusion Statistic and Equal Gain Combining Fusion Statistic, are proposed. [25] shows, in the case of weak signal, a comparison between a WSN with a FC receiving binary decisions that performs a Locally Most Powerful Test (LMPT) and the same network where the FC performs the LMPT after receiving the raw local measurements. In [26], [27] the Rao Test is proposed showing the asymptotically equivalent performances of this CR with respect to the Generalized Likelihood Ratio Test (GLRT). In [28] a set of fusion rules based on the GLRT, the Bayesian frameworks and hybrid approaches are shown; the work then proposes some fusion rules based on the Locally-Optimum Detection (LOD) framework; the paper also gives a basis for the localization of the target. The detection problem in WSN has also been approached proposing Multiple-Input Multiple-Output (MIMO) architectures with sensors sending local binary decisions to a FC where the focus is on the performance of the communication channel between sensors and FC [29]–[31].

The target localization problem in WSN with one FC and 1-bit local decisions has been studied in various works and several localization algorithms have been proposed. Many methods having a statistical basis can be found in [28]. Unfortunately, many of these methods have high computational complexity and have not been adapted or simplified to work in specific conditions like the one examined in this work. Statistical-based methods often require precise information on the statistical model of the signal which in many cases may not be available. As a consequence, several heuristic strategies have been developed that have the advantage of often having low computational complexity and easy implementation and requiring little knowledge on the statistical model of the signal. The most popular heuristic models are here reported. In [32] the centroid method is introduced showing great simplicity; this method has been subject to many variations to improve its performances reducing the ease of implementation and increasing the required knowledge on the statistical model of the signal turning it into range-based methods as in [33], [34], where the additional knowledge is used to create weights for the centroid calculation. Other popular range-free heuristic localization methods are the Center of the Minimum Enclosing Rectangle (CMER) [32] including its extension where the Steiner center is introduced to remove the dependency on the chosen coordinate system of the CMER [35], and the Center of

the Minimum Enclosing Circle (CMEC) [36]. Moreover, [32] shows the validity of the CMEC when sensors operate in noise-free settings with a unitary probability of detection in the proximity of the target.

An important aspect regarding WSNs with FC receiving 1-bit local decisions is the quantizer design. In [37] the local quantization problem is addressed for the problem of Bayesian estimation of location parameter in the case of a conditionally unbiased and efficient estimator with conditionally independent observations. The study is also extended to a scenario when the WSN is under a bit rate constraint and when the observations are conditionally dependent. In [38] the quantization task is treated for the problem of tracking moving targets showing a method for updating dynamically the local thresholds via Multiobjective Optimization Problem resulting in a trade-off solution between maximum Fisher Information and minimum sum of sensor transmission probabilities. The problem has also been treated for the detection task: in [39] the quantizers have been designed for a WSN performing a Generalized LOD (from Davies' framework) test for detection of a target whose position and emitted power is unknown; in this scenario the quantizers are designed using a semi-theoretical asymptotically optimal approach. In [40] it is shown the optimal quantizer in case of a deterministic signal and a WSN with imperfect reporting channel and a FC performing a GLRT concluding that the optimal threshold should be set to zero at all nodes. In [25] the case resulting quantizer was obtained through maximization of the Fisher Information. In [41] the binary asymmetric quantizer is obtained minimizing the maximum Cramér-Rao Lower Bound (CRLB) quantizer.

In general, the problem of the quantizer design has been mainly treated separately for the detection and estimation problem so that no optimal quantization strategy has been proposed so far to jointly maximize detection and parameter estimation performances.

B. Contribution and Paper Organization

This work investigates the use of a WSN made of passive acoustic sensors as an external LDS proposing two different methodologies for leak detection and four algorithms for leak localization and illustrates results on a realistic case-study based on the Goliat FPSO and represents a continuation and extension of the previous work on this topic [42], [43]. The underwater sensors transmit to the FC their decision regarding the presence or absence of a leakage assuming an On-Off Keying (OOK) modulation. The FC fuses the local decision and takes a global decision and, in the case that a leak is detected, estimates its position.

The detection is treated at sensor level showing the optimal test statistics to be performed locally, and at a global level, showing two fusion rules: the well-known CR, and a newly proposed modified version of the CVR (MCVR). The threshold selection is based on the optimization of an objective function and exploits the knowledge of the failure rates of the components of the SPS.

The analyzed localization methods can be divided into heuristic and Bayesian methods. The heuristic methods consist of a centroid-based algorithm, and a newly proposed modified

centroid-based algorithm representing an alteration of the first methods which extends the localization area without altering the complexity of the algorithm. The two proposed Bayesian algorithms are a *Maximum A-Posteriori* (MAP) estimator and a *Minimum Mean Square Error* (MMSE) estimator which are adapted to work in the current framework: they use the information of the failure rates of the components of the SPS to build the prior probabilities for these components being the leak source.

The present work shows some new advances in the field of process monitoring:

- The entire work is based on the knowledge and integration of reliability data of the SPS into the design and configuration of the LDS;
- The proposed algorithms are built keeping low computational complexity, and ease of implementation;
- The newly proposed MCVR offers, without altering the computational complexity of the CR, more flexibility and the possibility of better results;
- The modified centroid-based method for localization, without altering the computational complexity of the centroid-based method, removes the limitation imposed by a centroid of being located inside the smallest convex volume inscribing all the sensors;
- The proposed Bayesian localization algorithms are designed for increased performances keeping contained their complexity and can further exploit the knowledge of some reliability data of the SPS.

The remainder of the paper is organized as follows. Sec. II provides a system overview, focusing on the network architecture, the signal model (including assumptions related to signals characterizations), and the necessary knowledge on the SPS. Data processing for leak detection is described in Sec. III, which includes local detection at sensor location and global detection at the FC, plus a description of the methodology for the selection of the thresholds. Sec. IV shows the necessary steps of four proposed algorithms for leak localization. Numerical results on the considered case study are presented in Sec. V in terms of Receiver Operating Characteristic (ROC) for the detection and Root Mean Square Error (RMSE) for the localization. Finally, conclusions and further works are addressed in Sec. VI.

C. Notation

Upper-case bold letters denote matrices and lower-case bold letters denote column vectors; $(\cdot)^T$, and $\| \cdot \|$ denote transpose and Euclidean norm operators, respectively; $\hat{a}$ and $\mathbb{E}(a)$ denote an estimate and the expectation of the random variable a, respectively; $\Pr(\cdot)$ and $p(\cdot)$ denote probability mass functions (pmfs) and probability density functions (pdfs), while $\Pr(\cdot|\cdot)$ and $p(\cdot|\cdot)$ their corresponding conditional counterparts; $\mathcal{N}(\mu, \sigma^2)$ denotes a Gaussian distribution with mean μ and variance σ^2; $\mathcal{Q}(\cdot)$ is the complementary cumulative distribution function (ccdf) of the standard normal distribution; $\mathcal{B}(p)$ denotes a Bernoulli distribution with mean p and variance $p(1-p)$; the symbol $\sim$ means "distributed as"; $\delta(\cdot)$ is the Dirac delta function; $\binom{n}{k} = \frac{n!}{k!(n-k)!}$ denotes the binomial coefficient; finally $\mathcal{O}(\cdot)$ denotes the big O notation.
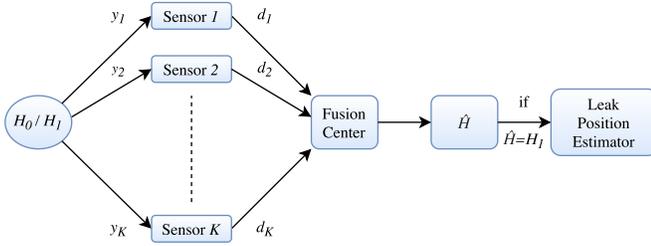
Fig. 1. Distributed Wireless Sensor Network.

II. SYSTEM MODEL

A. Distributed Wireless Sensor Network Architecture

The proposed distributed WSN architecture (see Fig. 1) is made of K passive acoustic sensors and one FC. The sensors sense sound pressure to detect the presence ($\mathcal{H}_1$) or absence ($\mathcal{H}_0$) of an oil spill.[1] The kth sensor (where $k = 1, 2, \ldots, K$) individually performs a test on the received signal y_k and takes a local decision $d_k = i \in \{0, 1\}$ if $\mathcal{H}_i$ is declared. The vector of local decisions $\boldsymbol{d} = \begin{bmatrix} d_1 \ldots d_K \end{bmatrix}^T$ is collected and processed at the FC for a global decision $\widehat{\mathcal{H}} \in \{\mathcal{H}_0, \mathcal{H}_1\}$. If $\widehat{\mathcal{H}} = \mathcal{H}_1$, the FC executes a localization algorithm to estimate the leak position. In addition to be spectrally-efficient, as only 1-bit communication is required on the reporting channel between the sensor and the FC, such a system is extremely energy efficient when OOK is employed for communicating the local decisions.

B. Signal Model

The model of the received sound pressure $y_k[n]$ at the kth sensor during the nth discrete time, depending on the corresponding hypothesis (absence/presence of a leakage), is the following:

$$\begin{cases} \mathcal{H}_0: & y_k[n] = w_k[n] \\ \mathcal{H}_1: & y_k[n] = \xi \, g(\boldsymbol{s}_k, \boldsymbol{\theta}) + w_k[n] \end{cases}, \quad (1)$$

where $\xi \sim \mathcal{N}(0, \sigma_\xi^2)$ and $w_k[n] \sim \mathcal{N}(0, \sigma_w^2)$ represent the emitted sound pressure produced by the leakage at a reference length (ℓ_{ref}) and the Additive White Gaussian Noise (AWGN), respectively. $w_k[n]$ and ξ are assumed both statistically independent due to the spatial separation of the sensors. The signal power σ_ξ^2 and the noise power σ_w^2 are assumed to be known, where σ_w^2 is assumed equal for all sensors. Also, $g(\boldsymbol{s}_k, \boldsymbol{\theta})$ represents the Amplitude Attenuation Function (AAF) depending on the distance between the kth sensor and the leak, whose positions are denoted $\boldsymbol{s}_k$ and $\boldsymbol{\theta}$, respectively. Here the AAF is treated as the contribution of the seawater absorption and the geometrical spreading and has the following form:

$$g(\boldsymbol{s}_k, \boldsymbol{\theta}) = \sqrt{\left(\frac{\ell_{\text{ref}}}{\|\boldsymbol{s}_k - \boldsymbol{\theta}\|}\right)^{k_{\text{sc}}} 10^{(\ell_{\text{ref}} - \|\boldsymbol{s}_k - \boldsymbol{\theta}\|)\alpha 10^{-4}}}, \quad (2)$$

where ℓ_{ref} and $\|\boldsymbol{s}_k - \boldsymbol{\theta}\|$ are measured in meters, the seawater absorption coefficient α is measured in [dB/km], and k_{sc} is the spreading coefficient. It can be noticed that if $\|\boldsymbol{s}_k - \boldsymbol{\theta}\| = \ell_{\text{ref}}$, then $g(\boldsymbol{s}_k, \boldsymbol{\theta}) = 1$. Any additional phenomenon influencing

[1]The analysis related to the sampling frequency is not considered in the present work.

the attenuation can only be modeled if the environmental conditions and the design of the SPS are precisely known. The seawater absorption coefficient α can be computed using several methods, e.g. *Thorp equation* [44], *Schulkin & Marsh equation* [45], *Fisher & Simmons equation* [46], *Ainslie & McColm equation* [47], and *Francois & Garrison equation* [48], [49]. The *Francois & Garrison equation*, reported in Appendix A is chosen in this work as it is one of the most performing equations available with one of the highest range of validity [50]. This equation depends on several variables such as salinity, reference frequency, temperature, depth, pH, and speed of sound. The underwater speed of sound, unlike the other variables, is often not available in form of experimental data, therefore it needs to be calculated numerically using one of the several equations available, e.g. *Medwin equation* [51], *Mackenzie equation* [52], *Del Grosso equation* [53], and *Chen & Millero equation* [54], [55]. In this work we choose to use the *Chen & Millero equation* with updated coefficients [56] due to its wide range of applicability [50]. This equation depends on variables such as salinity, temperature, and pressure (which can be obtained when depth and average seawater density are known) and is reported in Appendix B.

C. Subsea Production System

The SPS, as any plant, presents pieces of equipment and mechanical parts having higher failure rates which makes them more likely to cause a leakage. In this work, such components will be referred to as *hotspots*, and the position of the mth hotspot will be denoted $\boldsymbol{h}_m$ (where $m = 1, 2, \ldots, M$). We assume that the component failures are statistically independent and we denote φ_m the conditional probability (given the hypothesis $\mathcal{H}_1$) that a failure happens at the mth hotspot, which can be expressed as

$$\varphi_m = \Pr(\boldsymbol{\theta} = \boldsymbol{h}_m | \mathcal{H}_1) = \frac{f_m}{\sum\limits_{m=1}^{M} f_m}, \quad (3)$$

where f_m is the failure rate of the mth hotspot.

III. LEAK DETECTION

A. Local Detection

Given Eq. (1), the *uniformly most powerful* test [57] to be performed by the kth sensor at the generic nth instant is the energy test [28]:

$$d_k[n] = \begin{cases} 0, & y_k^2[n] < \tau_k \\ 1, & y_k^2[n] \geq \tau_k \end{cases}, \quad (4)$$

where τ_k is a local threshold. The local performances, in terms of probability of detection and probability of false alarm, of this test are defined and computed as follows:

$$P_{D,k} = \Pr(y_k^2[n] \geq \tau_k | \mathcal{H}_1) = 2\mathcal{Q}\left(\sqrt{\frac{\tau_k}{\sigma_\xi^2 g^2(\boldsymbol{s}_k, \boldsymbol{\theta}) + \sigma_w^2}}\right), \quad (5)$$

$$P_{F,k} = \Pr(y_k^2[n] \geq \tau_k | \mathcal{H}_0) = 2\mathcal{Q}\left(\sqrt{\frac{\tau_k}{\sigma_w^2}}\right). \quad (6)$$

However, since the leakage position is unknown, Eq. (5) cannot be used directly. One possibility to overcome this issue is to refer to average performances with respect to the SPS's hotspots, i.e.

$$\overline{P_{D,k}} = \sum_{m=1}^{M} \varphi_m P_{D,k,m} , \tag{7}$$

where $P_{D,k,m}$ is obtained replacing $\boldsymbol{\theta}$ with $\boldsymbol{h}_m$ in Eq. (5), with the implicit assumption that leakages generated in the different hotspots produce signals with equal power σ_ξ^2.

We define the reference Signal-to-Noise ratio (SNR) and the average sensing SNR at the kth sensor respectively as

$$\Gamma_{\mathrm{ref}} = \frac{\sigma_\xi^2}{\sigma_w^2} , \quad \Gamma_k = \Gamma_{\mathrm{ref}} \sum_{m=1}^{M} \varphi_m g^2(\boldsymbol{s}_k, \boldsymbol{h}_m) . \tag{8}$$

B. Global Detection

The FC assesses the presence of a leakage based on a test statistic (Λ) depending on the local decisions d_k (in this subsection we omit the dependence on n to keep notation short):

$$\widehat{\mathcal{H}} = \begin{cases} \mathcal{H}_0, & \Lambda < \tau_o \\ \mathcal{H}_1, & \Lambda \geq \tau_o \end{cases}, \tag{9}$$

where τ_o is a global threshold.

Three different fusion rules are considered for computing the test statistic at the FC: (i) the CR, (ii) the CVR, and (iii) the MCVR.

More specifically, the corresponding test statistics are computed as follows:

$$\Lambda_{\mathrm{CR}} = \sum_{k=1}^{K} d_k, \tag{10}$$

$$\Lambda_{\mathrm{CVR}} = \sum_{k=1}^{K} \left[d_k \ln\left(\frac{P_{D,k}}{P_{F,k}}\right) + (1 - d_k) \ln\left(\frac{1 - P_{D,k}}{1 - P_{F,k}}\right) \right], \tag{11}$$

$$\Lambda_{\mathrm{MCVR}} = \sum_{k=1}^{K} \left[d_k \ln\left(\frac{\overline{P_{D,k}}}{P_{F,k}}\right) + (1 - d_k) \ln\left(\frac{1 - \overline{P_{D,k}}}{1 - P_{F,k}}\right) \right]. \tag{12}$$

The CVR, obtained as the result of Log-Likelihood Ratio Test, is the optimal test statistics at the FC and results in the CR in the particular case where the sensors have equal local probabilities of detection and false alarm [20]. Unfortunately, the CVR cannot be used in its form as it requires knowledge of the $P_{D,k}$'s. For this reason the MCVR here proposed replaces $P_{D,k}$ with $\overline{P_{D,k}}$, via Eq. (7), for all k which are available. The computational complexity of both fusion rules (CR and MCVR) is $\mathcal{O}(K)$. Global system performances for each fusion rule are expressed in terms of *Global Probability of Detection* and *Global Probability of False Alarm* at the FC, defined respectively as $Q_D = \Pr(\Lambda \geq \tau_o|\mathcal{H}_1)$ and $Q_F = \Pr(\Lambda \geq \tau_o|\mathcal{H}_0)$. It is worth noticing that Q_D will depend on the leak

position, then the same approach used in Sec. III-A for local performances is considered here, i.e.

$$\overline{Q_D} = \sum_{m=1}^{M} \varphi_m Q_{D,m} . \tag{13}$$

C. Threshold Selection

Local thresholds τ_k are hyper-parameters that ideally should be optimized based on the global performance. Such a task does not exhibit an easy solution, then sub-optimal approaches are usually considered. In this work, thresholds selection is based on the maximization of the Youden's Index (J) [58]:

$$\tau^* = \arg\max_\tau J(\tau) = \arg\max_\tau \left\{ P_D(\tau) - P_F(\tau) \right\} . \tag{14}$$

In Eq. (14), the variables τ, P_D, and P_F are replaced with τ_k, $\overline{P_{D,k}}$, and $P_{F,k}$ when tuning the sensors, while they are replaced with τ_o, $\overline{Q_D}$, and Q_F when tuning the FC.

When tuning the FC, from a practical point of view, the number of thresholds is finite and their values can be obtained as follows (due to d_k in Eqs. (10) and (12) being binary):

- *CR case* – The CR exhibits a simple behavior; the set of possible thresholds is $\{0, 1, \ldots, K\}$ as these are the possible outcomes of Λ_{CR}. The number of possible thresholds is the number of K-combinations with repetitions of 2 elements (since the local decisions are binary):

$$C_{2,K} = \binom{(2+K)-1}{K} = K + 1 ; \tag{15}$$

- *MCVR case* – Being each sensor decision weighted with coefficients depending on the local performance, the number of possible thresholds is larger (unless all the coefficients happen to be equal). These thresholds can be obtained by computing all the possible outcomes of Λ_{MCVR}, given that the coefficients are known. The number of possible thresholds is the number of K-permutations with repetitions of 2 elements:

$$R_{2,K} = 2^K . \tag{16}$$

Note that the number of possible thresholds in the two cases includes also the threshold corresponding to the case in which $d_k = 0$ for all $k = 1, 2, \ldots, K$ resulting in $Q_D = Q_F = 1$.

IV. LEAK LOCALIZATION

Consequently to the detection of a leak, the FC provides an estimate of its position. In practical scenarios, a leakage happens at a certain (unknown) time denoted n_0 and remains in place for $n \geq n_0$ until maintenance is operated. Without loss of generality for the analysis of localization performance,[2] we assume $n_0 = 1$ with the leakage present all the time. In this work, four different algorithms are considered: (i) centroid-based localization, (ii) modified-centroid-based localization, (iii) MAP localization, and (iv) MMSE localization.

[2]It is worth repeating that our focus here is to assess the performance of the localization accuracy, while the assessment of early response of the system to a leakage usually analyzed within the framework of quickest detection [59] is beyond the scope of this work.

A. Centroid-Based Localization

This algorithm is based on the following steps:

1) Calculate the centroid of the sensors detecting a leakage at time n:

$$x^{(c)}[n] = \frac{\sum_{k=1}^{K} d_k[n]s_k}{\sum_{k=1}^{K} d_k[n]} \; ; \qquad (17)$$

2) Calculate the cumulative moving average (CMA) of the centroid positions based on Eq. (18);

$$\overline{x^{(c)}}[n]$$
$$= \begin{cases} x^{(c)}[1], & n=1 \\ \overline{x^{(c)}}[n-1] + \frac{1}{n}\left(x^{(c)}[n] - \overline{x^{(c)}}[n-1]\right), & n>1 \end{cases} \qquad (18)$$

3) Estimate the leak position via distance minimization between the positions of the hotspots and the CMA of the centroid:

$$m_o[n] = \arg\min_{m=1,\dots,M} \left\| \overline{x^{(c)}}[n] - h_m \right\|, \qquad (19)$$

$$\widehat{\theta}[n] = h_{m_o[n]} . \qquad (20)$$

B. Modified Centroid-Based Localization

This algorithm is proposed as the centroid-based algorithm does not allow the localization of those leakages happening in hotspots located outside the smallest convex volume inscribing all K sensors. This can be overcome through the modification of Eq. (17). The heuristic is to have, for each sensor not detecting the spill, the antipodal point ($s_k^{(a)}[n]$) with respect to a point reflection with the centroid $x^{(c)}[n]$ being the point of inversion. Hence, for the kth sensor such that $d_k[n] = 0$:

$$s_k^{(a)}[n] = 2x^{(c)}[n] - s_k . \qquad (21)$$

Let us define z as the centroid of all sensors present in the WSN:

$$z = \frac{1}{K}\sum_{k=1}^{K} s_k . \qquad (22)$$

This operation is necessary to obtain a modified centroid that accounts for both the active sensors (via actual position) and inactive sensors (via antipodal position):

$$x^{(mc)}[n] = \frac{1}{K}\sum_{k=1}^{K}\left(d_k[n]s_k + (1 - d_k[n])s_k^{(a)}[n]\right)$$
$$= 2x^{(c)}[n] - z . \qquad (23)$$

The presence of the antipodal position makes it possible for the FC to localize leakages outside the sensor's perimeter. Although it is possible to perform this algorithm by substituting Eq. (17) in Step 1 of the centroid-based algorithm with Eq. (23), the next steps show a way to present the algorithm that highlights the relationship with the final result of the centroid-based algorithm:

1) Calculate z using Eq. (22) — Since this term is constant over time, this step does not need to be repeated;
2) Calculate $x^{(c)}[n]$ as in Eq. (17);
3) Calculate a modified version of Eq. (18) using Eq. (24), which consists of the CMA of the modified centroid from Eq. (23);

$$\overline{x^{(mc)}}[n]$$
$$= \begin{cases} 2x^{(c)}[1] - z, & n=1 \\ 2\overline{x^{(c)}}[n-1] + \frac{2}{n}\left(x^{(c)}[n] - \overline{x^{(c)}}[n-1]\right) - z, & n>1 \end{cases} \qquad (24)$$

4) Estimate the leak position via distance minimization between the positions of the hotspots and the CMA of the modified centroid:

$$m_o[n] = \arg\min_{m=1,\dots,M} \left\| \overline{x^{(mc)}}[n] - h_m \right\|, \qquad (25)$$

$$\widehat{\theta}[n] = h_{m_o[n]} . \qquad (26)$$

C. Maximum A-Posteriori Localization

The following Bayesian estimator is proposed in order to exploit the prior knowledge of φ_m. This algorithm makes the simplification that $\Pr(\theta = h_m | d[n], \mathcal{H}_1) = \Pr(\theta = h_m | d[n], \widehat{\mathcal{H}} = \mathcal{H}_1)$:

1) For each hotspot, calculate of the log-likelihood of the decision vector at the nth discrete time $d[n]$ given that the leak is located in the mth hotspot using Eq. (27), as shown at the bottom of the page;
2) For each hotspot, compute the joint probability of the decision vectors up to the current discrete time via the updating formula in Eq. (28), as shown at the bottom of the page, where we have exploited conditional independence of sensors decision both in space and time;
3) Estimate the leak position chosen among the M hotspots through joint probability maximization:

$$m_o[n] = \arg\max_{m=1,\dots,M} \ln \Pr(d[1], \dots, d[n], \theta = h_m, \mathcal{H}_1), \qquad (29)$$

$$\widehat{\theta}[n] = h_{m_o[n]} . \qquad (30)$$

$$\ln \Pr(d[n] | \theta = h_m, \mathcal{H}_1) = \sum_{k=1}^{K}\left(d_k[n] \ln P_{D,k,m} + (1 - d_k[n]) \ln(1 - P_{D,k,m})\right) \qquad (27)$$

$$\ln \Pr(d[n], \dots, d[1], \theta = h_m, \mathcal{H}_1) = \begin{cases} \ln \Pr(d[1] | \theta = h_m, \mathcal{H}_1) + \ln \varphi_m, & n=1 \\ \ln \Pr(d[n] | \theta = h_m, \mathcal{H}_1) + \ln \Pr(d[n-1], \dots, d[1], \theta = h_m, \mathcal{H}_1), & n>1 \end{cases} \qquad (28)$$

D. Minimum Mean Square Error Localization

Also this Bayesian estimator is proposed to exploit the knowledge of φ_m, still relying on the simplification that $\Pr(\boldsymbol{\theta} = \boldsymbol{h}_m | \boldsymbol{d}[n], \mathcal{H}_1) = \Pr(\boldsymbol{\theta} = \boldsymbol{h}_m | \boldsymbol{d}[n], \widehat{\mathcal{H}} = \mathcal{H}_1)$. For compactness, let us introduce the following definition:

$$\alpha_m[n] \triangleq \Pr(\boldsymbol{d}[n], \ldots, \boldsymbol{d}[1], \boldsymbol{\theta} = \boldsymbol{h}_m, \mathcal{H}_1,) \ . \quad (31)$$

1) For each hotspot, calculate the likelihood of the decision vector at the nth discrete time $\boldsymbol{d}[n]$ given that the leak is located at the mth hotspot where we have exploited conditional independence of sensors decision in space;

$$\Pr(\boldsymbol{d}[n] | \boldsymbol{\theta} = \boldsymbol{h}_m, \mathcal{H}_1)$$
$$= \prod_{k=1}^{K} \left(P_{D,k,m}{}^{d_k[n]} (1 - P_{D,k,m})^{1-d_k[n]} \right) ; \quad (32)$$

2) Compute the geometric mean of all the probabilities $\Pr(\boldsymbol{d}[n] | \boldsymbol{\theta} = \boldsymbol{h}_m, \mathcal{H}_1)$ with $m = 1, \ldots, M$:

$$c_n = \left(\prod_{m=1}^{M} \Pr(\boldsymbol{d}[n] | \boldsymbol{\theta} = \boldsymbol{h}_m, \mathcal{H}_1) \right)^{1/M} ; \quad (33)$$

3) For each hotspot, compute the scaled version of the joint probability $\alpha_m[n]$ via the updating formula in Eq. (34);

$$\tilde{\alpha}_m[n]$$
$$= \begin{cases} \varphi_m, & n = 0 \\ c_n^{-1} \Pr(\boldsymbol{d}[n] | \boldsymbol{\theta} = \boldsymbol{h}_m, \mathcal{H}_1) \tilde{\alpha}_m[n-1], & n > 0 \end{cases}$$
$$(34)$$

4) Calculate the expected value of the posterior probability of the leak position given the decisions vectors up to the current discrete time (proof is reported in Appendix C):

$$\boldsymbol{x}^{(\text{mmse})}[n] = \mathbb{E}(\boldsymbol{\theta} | \boldsymbol{d}[n], \ldots, \boldsymbol{d}[1], \mathcal{H}_1)$$
$$= \frac{\sum_{m=1}^{M} \tilde{\alpha}_m[n] \boldsymbol{h}_m}{\sum_{m=1}^{M} \tilde{\alpha}_m[n]} ; \quad (35)$$

5) Estimate the leak position via distance minimization between the positions of the hotspots and the result of Eq. (35):

$$m_o[n] = \underset{m=1,\ldots,M}{\arg\min} \left\| \boldsymbol{x}^{(\text{mmse})}[n] - \boldsymbol{h}_m \right\| , \quad (36)$$

$$\widehat{\boldsymbol{\theta}}[n] = \boldsymbol{h}_{m_o[n]} . \quad (37)$$

A normalization procedure like that reported in Steps 2 and 3 is required to avoid arithmetic underflow for sufficiently large values of n. A proper normalization coefficient can be found computing a log-average of the values (by averaging their natural logarithms and then performing the exponential to return to the original scale), which is equivalent to their geometric mean. This has the benefit to properly scale all likelihoods of the observations of the sensors at each instant avoiding an unwanted underflow.

TABLE I
COMPUTATIONAL COMPLEXITY OF THE PROPOSED
LEAK LOCALIZATION ALGORITHMS

| Localization Algorithm	Complexity
Centroid-Based	$\mathcal{O}(K+M)$
Modified Centroid-Based	$\mathcal{O}(K+M)$
Maximum A-Posteriori	$\mathcal{O}(KM)$
Minimum Mean Square Error	$\mathcal{O}(KM)$
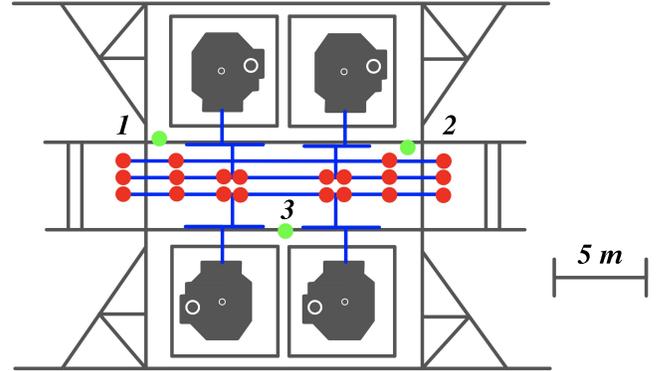
Fig. 2. Goliat's subsea template: the grey elements are the structure and the subsea trees, the blue lines constitutes the manifold, the green dots are the passive acoustic sensors, and the red dots are the hotspots.

Table I compares the computational complexity of the proposed leak localization algorithms.

V. CASE STUDY — GOLIAT FPSO

The Goliat FPSO is an oil production platform located in the Norwegian Barents Sea and it is currently the world's northernmost offshore platform. Because of its location in an environmentally sensitive area, the platform is subject to strict regulations, especially regarding oil spills. The Goliat FPSO employs a SPS which relies on 8 subsea templates for a total of 22 wells (12 production wells, 7 water injectors, and 3 gas injectors). Each template is equipped with a manifold and four well slots as shown in Fig. 2. The LDS monitoring each template is a combination of internal and external sensors, although the main usage of the internal sensors is process monitoring. Regarding the external LDS, one capacitive sensor is positioned above each subsea tree, while $K = 3$ passive acoustic sensors are installed to monitor the manifold [60], [61]. It is important to mention that the installed LDS is mainly designed to carry out the detection task, not the localization task being this one less critical. $M = 20$ hotspots have been recognized after a reliability analysis on the SPS. Such components correspond to 14 valves (8 branch valves and 6 isolation valves) and 6 connectors (4 connecting production lines and 2 connecting gas lift lines). Sensors and hotspots are highlighted in Fig. 2 where it can be seen that 6 (resp. 14) hotspots being inside (resp. outside) the sensors' perimeter. According to the OREDA (Offshore and Onshore Reliability Data) Handbook, the failure rates of connectors and isolation valves (in subsea manifolds) have the same order of magnitude ($10^{-6}\,\text{h}^{-1}$) giving no specific

TABLE II
PARAMETERS USED TO SIMULATE A LEAK SCENARIO

Parameter	Value	Note / Reference
Reference Frequency	2.5 kHz	[13]
Temperature	3.8 °C	[63]
Salinity	35 ‰	[63]
Depth	350 m	[60]
pH	8	[64]
Spreading Coefficient (k_{sc})	1.5	[65]
Reference Length (ℓ_{ref})	1 m	–
Noise Variance (σ_w^2)	1	–
φ_m	$1/M$	$f_1 = f_2 = \ldots = f_M$
Γ_{ref}	10 dB; 15 dB	–

TABLE III
AVERAGE SENSING SNR AT THE DIFFERENT SENSORS

| Γ_{ref}	Γ_1	Γ_2	Γ_3
10 dB	−0.63 dB	0.39 dB	−1.61 dB
15 dB	4.37 dB	5.39 dB	3.39 dB
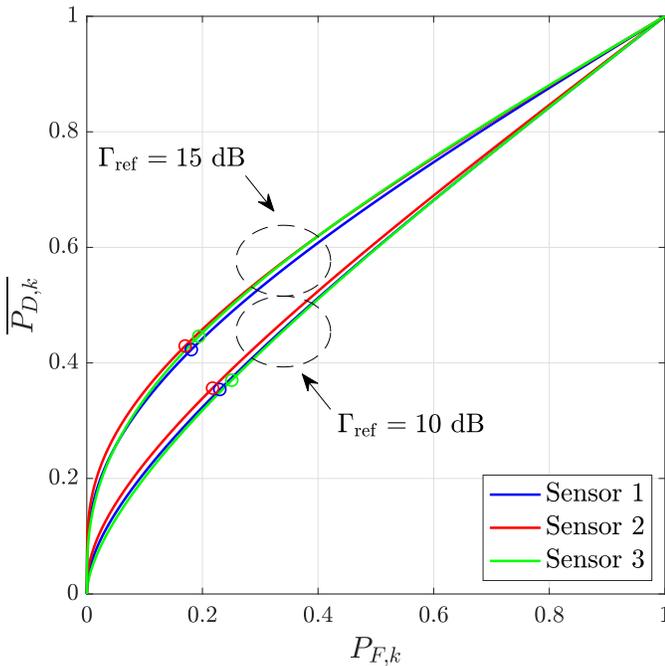
Fig. 3. Local ROC curves highlighting the operating points selected via Youden's Index maximization.

values based on the different diameters or other design specifications [62]. As a consequence, we can assume the hotspots to have the same value of f_m. In the case study, hotspots and sensors are assumed to be at the same height.

The methodologies for detection and localization described in the previous sections are applied here assuming that the sensors are part of a WSN as described in Sec. II.

In order to better analyze the results, two different cases are simulated: $\Gamma_{ref} \in \{10\,\text{dB}, 15\,\text{dB}\}$.

The values of $\overline{Q_D}$ and Q_F have been computed via numerical simulation with 10^8 Monte Carlo runs equally divided

TABLE IV
LEAK DETECTION PERFORMANCES AT THE SENSORS

| Γ_{ref}	Sensor (k)	τ_k^*	$\overline{P_{D,k}}(\tau_k^*)$	$P_{F,k}(\tau_k^*)$	$J(\tau_k^*)$
10 dB	1	1.4402	0.3540	0.2301	0.1238
	2	1.5204	0.3563	0.2176	0.1388
	3	1.3189	0.3701	0.2508	0.1193
15 dB	1	1.7916	0.4230	0.1807	0.2422
	2	1.8820	0.4293	0.1701	0.2592
	3	1.6887	0.4460	0.1938	0.2522
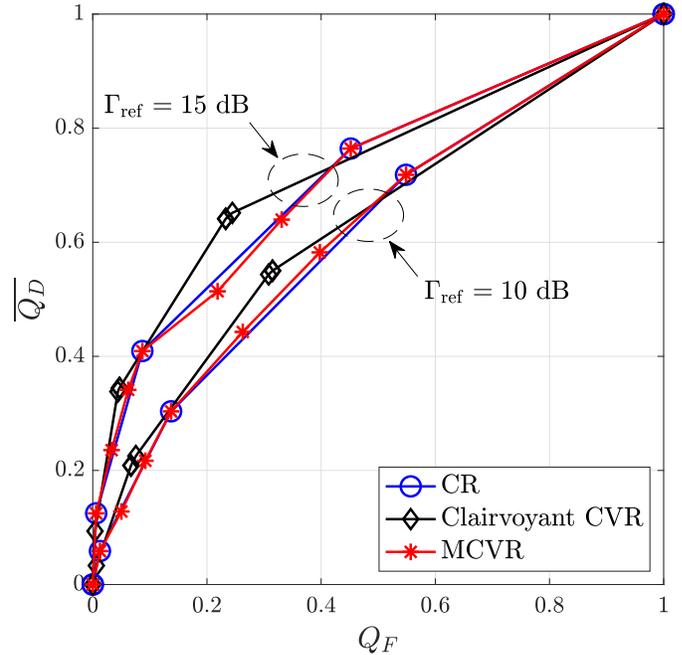
Fig. 4. Global ROC curves.

between $\mathcal{H}_0$ and $\mathcal{H}_1$. The localization performances have been produced via numerical simulation with 10^4 Monte Carlo runs where the $\mathcal{H}_1$ scenario is simulated. The simulation is carried out with the FC performing both the CR and the MCVR operating at the thresholds obtained via maximization of the Youden's Index. The performances are assessed in terms of variation of the RMSE with respect to the number of instants (N) since the leakage started occurring. All the simulations have been carried out using the software MATLAB. The parameters used for the case study are found in Table II.

A. Local Detection Results

Table III shows the average SNR for each sensor in the case of $\Gamma_{ref} = 10$ dB and $\Gamma_{ref} = 15$ dB obtained via Eq. (8).

Table IV shows the tuning result after the maximization of the local Youden's Index which highlights how a higher value of Γ_k allows a higher resulting threshold τ_k^*. In this specific scenario sensor 2 has the highest value of Γ_k for both Γ_{ref}. The location of the operating points in the ROC space can be seen in Fig. 3 where it can be noticed that the averaging procedure in Eq. (7) provides 3 similar ROC curves, leading to similar operating points.
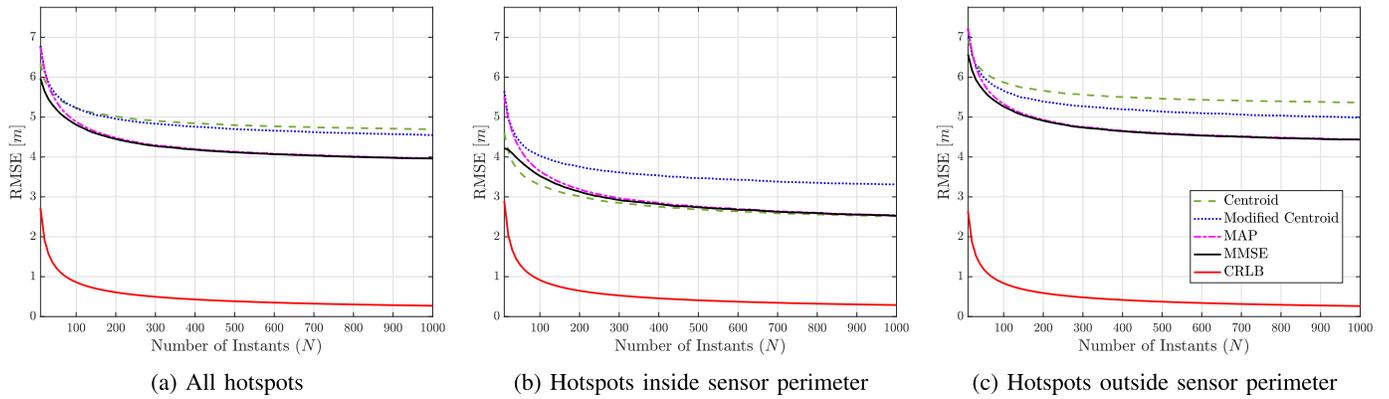
Fig. 5. Localization performance with CR and $\Gamma_{\text{ref}} = 10\,\text{dB}$.

This behavior is not surprising as this case study shows sufficiently similar values of Γ_k. The impact of efficient sensor placement, possible through the maximization of Γ_k for each sensor, is not investigated in this work.

B. Global Detection Results

Fig. 4 shows the ROC curves of the LDS in the two cases comparing the CR and the MCVR using the (position) Clairvoyant CVR as upper bound (enabling the use of Eq. (11)). The impact of Γ_{ref} on the global performance is apparent. The ROC curves of the two different fusion rules are largely similar, thus each operation point of the CR might be achieved also with the MCVR via appropriate threshold selection. Excluding the useless cases with $\overline{Q_D} = Q_F = 0$ and $\overline{Q_D} = Q_F = 1$, based on Eq. (15) and Eq. (16) the CR (resp. the MCVR) provides 3 (resp. 7) possible operation points, thus the large flexibility of the MCVR allows to take into account for more design needs with respect to the CR. On the other hand, the Clairvoyant CVR shows a different behavior since its points do not overlap with those generated by the two fusion rules. Note that in Fig. 4 the curves of the MCVR and the CR cross the curve of the Clairvoyant CVR in certain areas of the plot. This should not surprise as the lines are simple linking segments between points representing two consecutive thresholds and must not be interpreted as a continuous locus of possible operation points.

Table V shows the operation points from the threshold optimization procedures. Both CR and MCVR show lower values of maximum Youden's Index when compared to the Clairoyant CVR. It is interesting to notice that in the case of high SNR (e.g. $\Gamma_{\text{ref}} = 15\,\text{dB}$), the optimal operation points from the two considered fusion rules are very similar, while for lower SNR values (e.g. $\Gamma_{\text{ref}} = 10\,\text{dB}$) the optimization points are different and the one from the MCVR has no counterpart with the CR, moreover, the optimization point from the MCVR in such scenario tends to be closer (in terms of $\overline{Q_D}$ and Q_F) to the one from the Clairvoyant CVR. This shows how the MCVR, maintaining the same complexity of the CR, gives more flexibility to the LDS and may enable better results.

C. Localization Results

Fig. 5, 6, 7, and 8 show the result of the four proposed localization techniques for both fusion rules (CR and MCVR)

TABLE V
LEAK DETECTION PERFORMANCES AT THE FC

Γ_{ref}	Fusion Rule	τ_o^*	$\overline{Q_D}(\tau_o^*)$	$Q_F(\tau_o^*)$	$J(\tau_o^*)$
	CR	1	0.7183	0.5487	0.1696
10 dB	Clairvoyant CVR	0.0849	0.5435	0.3081	0.2354
	MCVR	0.0650	0.5823	0.3977	0.1846
	CR	2	0.4093	0.0868	0.3225
15 dB	Clairvoyant CVR	0.1411	0.6411	0.2328	0.4083
	MCVR	1.3584	0.4092	0.0869	0.3224

and both reference SNR values ($\Gamma_{\text{ref}} = 10\,\text{dB}$ and $\Gamma_{\text{ref}} = 15\,\text{dB}$). In addition, the Cramér-Rao Lower Bound (CRLB) is displayed for an estimator that follows a perfect detector ($\overline{Q_D} = 1$, $Q_F = 0$). The derivation of the CRLB can be found in Appendix D. As a consequence, such CRLB is independent of the evaluated fusion rule and only depends on the value of Γ_{ref}. Clearly, such lower bound is purely theoretical and cannot be attained as a perfect detection cannot be achieved even in the case of the (position) Clairvoyant CVR (see Fig. 4). The different performance related to the case of a leakage located inside or outside the sensor perimeter is also highlighted. For the simulations, local and global thresholds in Table IV and Table V were considered.

Again, the figures show that even from the localization perspective, at high SNR (i.e. $\Gamma_{\text{ref}} = 15\,\text{dB}$) the corresponding localization procedures perform similarly independently of the considered fusion rule (CR or MCVR). Apparently, the centroid-based method is the least performing, as it fails in localizing leakages outside the sensor perimeter. The newly proposed modified-centroid-based method tackles this limitation through the reflection of the positions of the inactive sensors and the numerical simulations confirm the effectiveness of such approach, which does not require additional computational resources. It is worth highlighting that the centroid-based method is extremely well performing when leakages are located inside the sensor perimeter, but extremely bad-performing in the other cases.

Both the considered statistical approaches exhibit better performance than the previous heuristic ones, with a price in terms of computational complexity. More specifically, MAP and MMSE behave similarly, with the latter slightly outperforming the former when few samples are available.

(a) All hotspots

(b) Hotspots inside sensor perimeter

(c) Hotspots outside sensor perimeter
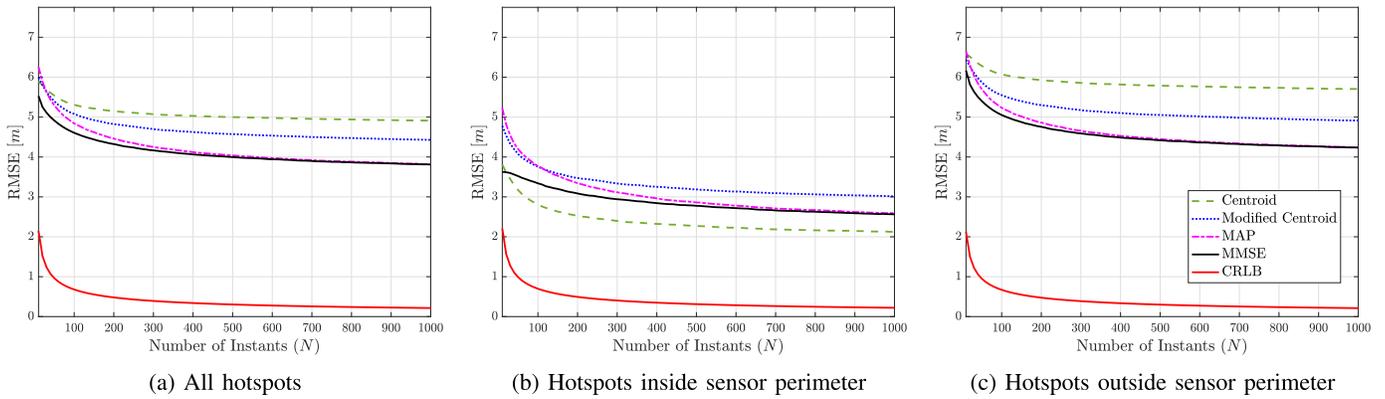
Fig. 6. Localization performance with CR and $\Gamma_{\text{ref}} = 15\,\text{dB}$.

(a) All hotspots

(b) Hotspots inside sensor perimeter

(c) Hotspots outside sensor perimeter
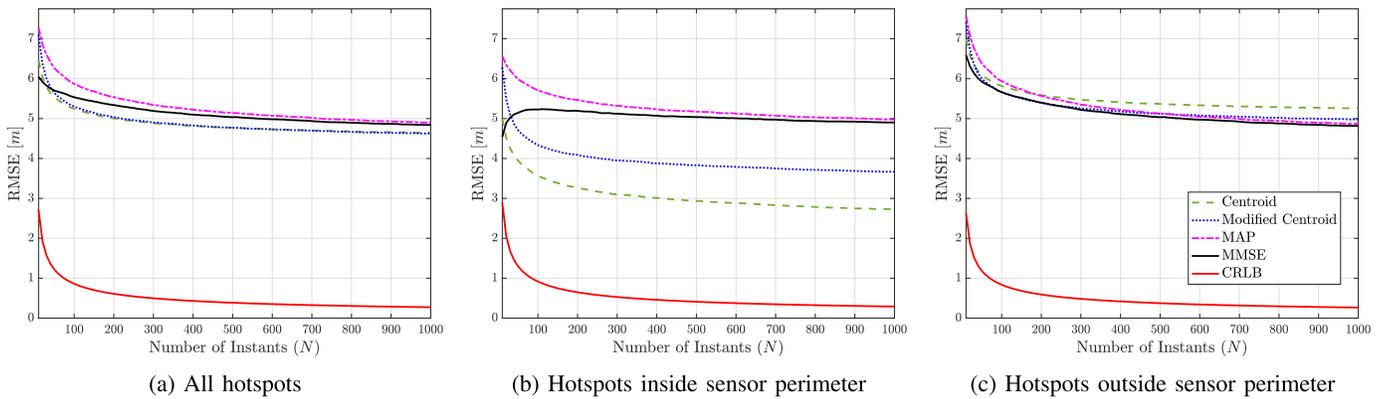
Fig. 7. Localization performance with MCVR and $\Gamma_{\text{ref}} = 10\,\text{dB}$.

(a) All hotspots

(b) Hotspots inside sensor perimeter

(c) Hotspots outside sensor perimeter
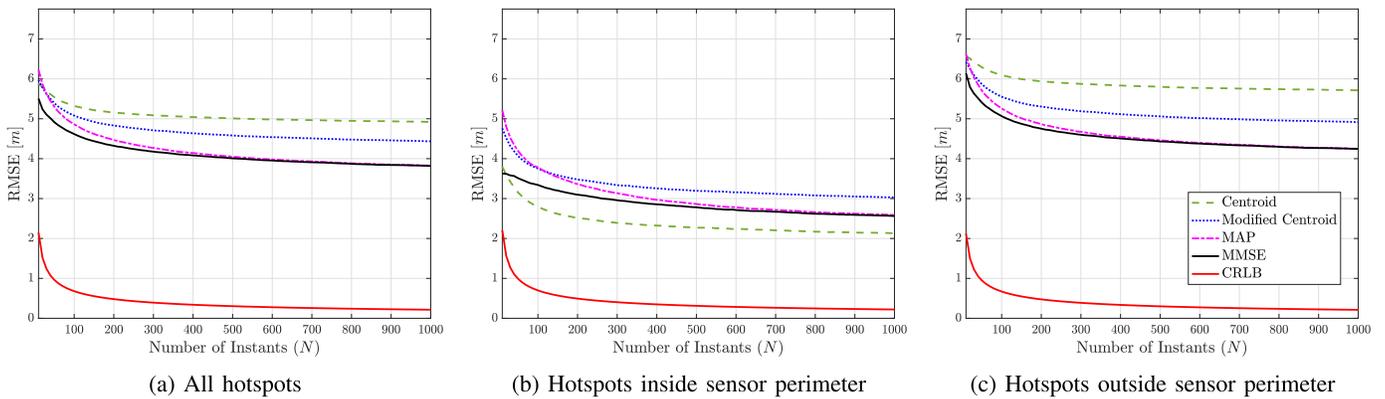
Fig. 8. Localization performance with MCVR and $\Gamma_{\text{ref}} = 15\,\text{dB}$.

The CRLB shows little variation when the target is inside the sensor perimeter compared to when it is located outside. Not surprisingly the CRLB, despite showing better performances in case $\Gamma_{\text{ref}} = 15$ dB for small values of N (the RMSE is around 1 meter smaller), converges to zero in both case as $N \to \infty$. This convergence is fast enough to make the difference in RMSE look imperceptible in the two cases at sufficiently high values of N.

Finally, it is worth mentioning that the trade-off between the probabilities of detection and false alarm at the detection stage is handled in this work through the Youden's Index maximization. However, from localization perspective, it is the detection probability that matters as localization performance increases with it. This must be considered when comparing performance related to different reference SNR which might correspond to different operation points of the ROC. The design of the overall parameters configuration taking into account both detection and localization performance is not considered in this work.

VI. CONCLUSION

This work investigated the use of WSNs for subsea oil spill detection and localization, using Goliat FPSO as a case study. Local sensors' binary decisions are collected at the FC, where

CR and MCVR are considered for data fusion. ROC performances, obtained through realistic numerical simulations, showed the potential benefit of the considered approach. Two heuristic and two Bayesian estimation algorithms have been considered for localization, with the second pair exhibiting better performance but higher computational complexity.

The proposed methodologies were developed taking into account a possible integration of the LDS with the DRMF, exploiting the results of a risk analysis carried out on the SPS. The detection and localization results show the benefit of designing a LDS exploiting the knowledge of the hotspots of the SPS and their failure rates as these help us computing prior probabilities to be used in the algorithms. A key element for a performing LDS is the integration of the results of the risk analysis into the LDS design in an iterative exchange of information to increase the system capability of predicting and handling unwanted events. Thresholds selection has been based on detection performance only, while future work would include localization performance into hyperparameters optimization and exploring the impact of system design on risk management.

APPENDIX A
FRANCOIS & GARRISON EQUATION

The following equation can be found in [48], [49]. This method requires that the input values are in the exact measurement units reported at the end of the Appendix.

Absorption Coefficient [dB km^{-1}]:

$$\alpha = \underbrace{\frac{A_1 P_1 f_1 f^2}{f^2 + f_1^2}}_{\substack{H_3BO_3 \\ \text{Contribution}}} + \underbrace{\frac{A_2 P_2 f_2 f^2}{f^2 + f_2^2}}_{\substack{MgSO_4 \\ \text{Contribution}}} + \underbrace{A_3 P_3 f^2}_{\substack{H_2O \\ \text{Contribution}}}$$

H_3BO_3 Contribution:

$$A_1 = \frac{8.86}{c} 10^{(0.78\,pH-5)} \left[\frac{dB}{km\,kHz}\right]$$

$$P_1 = 1$$

$$f_1 = 2.8\,(S/35)^{0.5}\,10^{[4-1245/(T+273)]}[kHz]$$

$MgSO_4$ Contribution:

$$A_2 = 21.44\,\frac{S}{c}\,(1 + 0.025\,T)\left[\frac{dB}{km\,kHz}\right]$$

$$P_2 = 1 - 1.37 \cdot 10^{-4}\,D + 6.2 \cdot 10^{-9}\,D^2$$

$$f_2 = \frac{8.17 \cdot 10^{[8-1990/(T+273)]}}{1 + 0.0018\,(S - 35)}[kHz]$$

H_2O Contribution:

$$A_3 = \sum_{m=0}^{3} a_m T^m \left[\frac{dB}{km\,kHz^2}\right]$$

$$P_3 = 1 - 3.83 \cdot 10^{-5}\,D + 4.9 \cdot 10^{-10}\,D^2$$

In the above-reported method f is the frequency [kHz], c is the speed of sound [m s^{-1}], S is the salinity [‰], T is the temperature [°C], and D is the depth [m]. The temperature-dependent values of the coefficients a_m ($m = 0, 1, 2, 3$) are reported in Tab. VI.

TABLE VI
COEFFICIENTS OF THE H$_2$O CONTRIBUTION

Temperature	$a_0 \cdot 10^4$	$a_1 \cdot 10^5$	$a_2 \cdot 10^7$	$a_3 \cdot 10^8$
$T \leq 20\,°C$	4.397	-2.59	9.11	-1.50
$T > 20\,°C$	3.964	-1.146	1.45	$-6.5 \cdot 10^{-2}$

TABLE VII
UPDATED COEFFICIENTS OF CHEN & MILLERO EQUATION

Coefficient	Value	Coefficient	Value
C_{00}	1402.388	A_{01}	$-1.262 \cdot 10^{-2}$
C_{01}	5.03830	A_{02}	$7.166 \cdot 10^{-5}$
C_{02}	$-5.81090 \cdot 10^{-2}$	A_{03}	$2.008 \cdot 10^{-6}$
C_{03}	$3.3432 \cdot 10^{-4}$	A_{04}	$-3.21 \cdot 10^{-8}$
C_{04}	$-1.47797 \cdot 10^{-6}$	A_{10}	$9.4742 \cdot 10^{-5}$
C_{05}	$3.1419 \cdot 10^{-9}$	A_{11}	$-1.2583 \cdot 10^{-5}$
C_{10}	0.153563	A_{12}	$-6.4928 \cdot 10^{-8}$
C_{11}	$6.8999 \cdot 10^{-4}$	A_{13}	$1.0515 \cdot 10^{-8}$
C_{12}	$-8.1829 \cdot 10^{-6}$	A_{14}	$-2.0142 \cdot 10^{-10}$
C_{13}	$1.3632 \cdot 10^{-7}$	A_{20}	$-3.9064 \cdot 10^{-7}$
C_{14}	$-6.1260 \cdot 10^{-10}$	A_{21}	$9.1061 \cdot 10^{-9}$
C_{15}	0	A_{22}	$-1.6009 \cdot 10^{-10}$
C_{20}	$3.1260 \cdot 10^{-5}$	A_{23}	$7.994 \cdot 10^{-12}$
C_{21}	$-1.7111 \cdot 10^{-6}$	A_{30}	$1.100 \cdot 10^{-10}$
C_{22}	$2.5986 \cdot 10^{-8}$	A_{31}	$6.651 \cdot 10^{-12}$
C_{23}	$-2.5353 \cdot 10^{-10}$	A_{32}	$-3.931 \cdot 10^{-13}$
C_{24}	$1.0415 \cdot 10^{-12}$	A_{33}	0
C_{25}	0	A_{34}	0
C_{30}	$-9.7729 \cdot 10^{-9}$	A_{24}	0
C_{31}	$3.8513 \cdot 10^{-10}$	B_{00}	$-1.922 \cdot 10^{-2}$
C_{32}	$-2.3654 \cdot 10^{-12}$	B_{01}	$-4.42 \cdot 10^{-5}$
C_{33}	0	B_{10}	$7.3637 \cdot 10^{-5}$
C_{34}	0	B_{11}	$1.7950 \cdot 10^{-7}$
C_{35}	0	D_{00}	$1.727 \cdot 10^{-3}$
A_{00}	1.389	D_{10}	$-7.9836 \cdot 10^{-6}$

APPENDIX B
CHEN & MILLERO EQUATION

The following equation can be found in [54]. Table VII uses the updated coefficient present in [56] after the adoption of the International Temperature Scale of 1990. This method requires that the input values are in the exact measurement units reported at the end of the Appendix.

Speed of Sound:

$$c = C + AS + BS^{3/2} + DS^2$$

$$C = \sum_{m=0}^{3}\sum_{n=0}^{5} C_{mn} P^m T^n$$

$$A = \sum_{m=0}^{3}\sum_{n=0}^{4} A_{mn} P^m T^n$$

$$B = \sum_{m=0}^{1}\sum_{n=0}^{1} B_{mn} P^m T^n$$

$$D = D_{00} + D_{10} P$$

where c is the speed of sound [m s^{-1}], S is the salinity [‰], T is the temperature [°C], and P is the pressure [kPa]. The values of the coefficients C_{mn}, A_{mn}, B_{mn}, and D_{mn} are reported in Tab. VII.

APPENDIX C
PROOF OF MMSE ALGORITHM

Here we show the validity of Eq. (35) exploiting the conditional independence of sensors decision in time:

$$
\begin{aligned}
&\boldsymbol{x}^{(\mathrm{mmse})}[n] \\
&= \mathbb{E}\left(\boldsymbol{\theta} | \boldsymbol{d}[n], \ldots, \boldsymbol{d}[1], \mathcal{H}_1\right) \\
&= \int p(\boldsymbol{\theta} | \boldsymbol{d}[n], \ldots, \boldsymbol{d}[1], \mathcal{H}_1) \boldsymbol{\theta} \, \mathrm{d}\boldsymbol{\theta} \\
&= \int \frac{p(\boldsymbol{d}[n], \ldots, \boldsymbol{d}[1] | \boldsymbol{\theta}, \mathcal{H}_1) p(\boldsymbol{\theta} | \mathcal{H}_1)}{p(\boldsymbol{d}[n], \ldots, \boldsymbol{d}[1] | \mathcal{H}_1)} \boldsymbol{\theta} \, \mathrm{d}\boldsymbol{\theta} \\
&= \frac{\int p(\boldsymbol{d}[n], \ldots, \boldsymbol{d}[1] | \boldsymbol{\theta}, \mathcal{H}_1) p(\boldsymbol{\theta} | \mathcal{H}_1) \boldsymbol{\theta} \, \mathrm{d}\boldsymbol{\theta}}{\int p(\boldsymbol{d}[n], \ldots, \boldsymbol{d}[1] | \boldsymbol{\theta}, \mathcal{H}_1) p(\boldsymbol{\theta} | \mathcal{H}_1) \, \mathrm{d}\boldsymbol{\theta}} \\
&= \frac{\sum_{m=1}^{M} \operatorname{Pr}(\boldsymbol{d}[n], \ldots, \boldsymbol{d}[1] | \boldsymbol{\theta} = \boldsymbol{h}_m, \mathcal{H}_1) \operatorname{Pr}(\boldsymbol{\theta} = \boldsymbol{h}_m | \mathcal{H}_1) \boldsymbol{h}_m}{\sum_{m=1}^{M} \operatorname{Pr}(\boldsymbol{d}[n], \ldots, \boldsymbol{d}[1] | \boldsymbol{\theta} = \boldsymbol{h}_m, \mathcal{H}_1) \operatorname{Pr}(\boldsymbol{\theta} = \boldsymbol{h}_m | \mathcal{H}_1)} \\
&= \frac{\left(\prod_{i=1}^{n} c_i^{-1}\right) \sum_{m=1}^{M} \left(\prod_{i=1}^{n} \operatorname{Pr}(\boldsymbol{d}[i] | \boldsymbol{\theta} = \boldsymbol{h}_m, \mathcal{H}_1)\right) \varphi_m \boldsymbol{h}_m}{\left(\prod_{i=1}^{n} c_i^{-1}\right) \sum_{m=1}^{M} \left(\prod_{i=1}^{n} \operatorname{Pr}(\boldsymbol{d}[i] | \boldsymbol{\theta} = \boldsymbol{h}_m, \mathcal{H}_1)\right) \varphi_m} \\
&= \frac{\sum_{m=1}^{M} c_n^{-1} \operatorname{Pr}(\boldsymbol{d}[n] | \boldsymbol{\theta} = \boldsymbol{h}_m, \mathcal{H}_1) \tilde{\alpha}_m[n-1] \boldsymbol{h}_m}{\sum_{m=1}^{M} c_n^{-1} \operatorname{Pr}(\boldsymbol{d}[n] | \boldsymbol{\theta} = \boldsymbol{h}_m, \mathcal{H}_1) \tilde{\alpha}_m[n-1]} \\
&= \frac{\sum_{m=1}^{M} \tilde{\alpha}_m[n] \boldsymbol{h}_m}{\sum_{m=1}^{M} \tilde{\alpha}_m[n]},
\end{aligned}
$$

where

$$
\begin{aligned}
&p(\boldsymbol{d}[n], \ldots, \boldsymbol{d}[1] | \boldsymbol{\theta}, \mathcal{H}_1) \\
&\quad = \sum_{m=1}^{M} \operatorname{Pr}(\boldsymbol{d}[n], \ldots, \boldsymbol{d}[1] | \boldsymbol{\theta} = \boldsymbol{h}_m, \mathcal{H}_1) \delta(\boldsymbol{\theta} - \boldsymbol{h}_m),
\end{aligned}
$$

and

$$
p(\boldsymbol{\theta} | \mathcal{H}_1) = \sum_{m=1}^{M} \operatorname{Pr}(\boldsymbol{\theta} = \boldsymbol{h}_m | \mathcal{H}_1) \delta(\boldsymbol{\theta} - \boldsymbol{h}_m).
$$

APPENDIX D
DERIVATION OF THE CRAMÉR-RAO LOWER BOUND

We derive the CRLB of an estimator $\widehat{\boldsymbol{\theta}}$ that follows a perfect detector ($\overline{Q_D} = 1, Q_F = 0$). In agreement with the case study, we consider $\boldsymbol{\theta}, \boldsymbol{s}_k, \boldsymbol{h_m} \in \mathbb{R}^2$, $\forall k = 1, \ldots, K$ and $\forall m = 1, \ldots, M$, although the procedure is analogous for the case of vectors belonging to $\mathbb{R}^3$.

The CRLB, for each component of $\widehat{\boldsymbol{\theta}} = \left[\widehat{\theta}_1 \ \widehat{\theta}_2\right]^T$, is based on the Fisher Information Matrix (FIM) $\boldsymbol{I}(\boldsymbol{\theta})$:

$$
CRLB\left(\widehat{\theta}_i\right) = [\boldsymbol{I}(\boldsymbol{\theta})]_{ii}^{-1}. \tag{38}
$$

The FIM is obtained exploiting its additive property for independent observations in space and time, i.e.

$$
\boldsymbol{I}(\boldsymbol{\theta}) = N \sum_{k=1}^{K} \boldsymbol{I}_k(\boldsymbol{\theta}), \tag{39}
$$

where $\boldsymbol{I}_k(\boldsymbol{\theta})$ is the FIM with respect to the local decisions of the kth sensor at the generic instant n, and N is the number of instants since the spill occurred (i.e. the number of performed estimations). The expression of $\boldsymbol{I}_k(\boldsymbol{\theta})$ is obtained as follows:

$$
\boldsymbol{I}_k(\boldsymbol{\theta}) = \mathbb{E}_{d_k[n] | \mathcal{H}_1}\left[\left(\frac{\partial \ln p(d_k[n] | \mathcal{H}_1; \boldsymbol{\theta})}{\partial \boldsymbol{\theta}}\right) \times \left(\frac{\partial \ln p(d_k[n] | \mathcal{H}_1; \boldsymbol{\theta})}{\partial \boldsymbol{\theta}}\right)^T\right],
$$

where

$$
\begin{aligned}
\frac{\partial \ln p(d_k[n] | \mathcal{H}_1; \boldsymbol{\theta})}{\partial \boldsymbol{\theta}} &= \frac{\partial}{\partial \boldsymbol{\theta}} \ln \left(P_{D,k}^{d_k[n]} (1 - P_{D,k})^{1 - d_k[n]}\right) \\
&= \frac{d_k[n] - P_{D,k}}{P_{D,k}(1 - P_{D,k})} \frac{\partial P_{D,k}}{\partial \boldsymbol{\theta}},
\end{aligned}
$$

and, using the definition of $P_{D,k}$ in Eq. (5),

$$
\begin{aligned}
\frac{\partial P_{D,k}}{\partial \boldsymbol{\theta}} &= p_{\mathcal{N}(0,1)}\left(\sqrt{\frac{\tau_k}{\sigma_\xi^2 g^2(u) + \sigma_w^2}}\right) \\
&\quad \times \frac{\sigma_\xi^2 \sqrt{\tau_k}}{\left[\sigma_\xi^2 g^2(u) + \sigma_w^2\right]^{3/2}} \frac{\partial \left(g^2(u)\right)}{\partial \boldsymbol{\theta}},
\end{aligned}
$$

with $u = \|\boldsymbol{s}_k - \boldsymbol{\theta}\|$. Also, the chain rule provides

$$
\frac{\partial \left(g^2(u)\right)}{\partial \boldsymbol{\theta}} = \frac{\partial \left(g^2(u)\right)}{\partial u} \frac{\partial u}{\partial \boldsymbol{\theta}} = \psi(u) \frac{\boldsymbol{\theta} - \boldsymbol{s}_k}{u}
$$

where, using the definition of $g(u)$ in Eq. (2),

$$
\psi(u) = \frac{\partial \left(g^2(u)\right)}{\partial u} = -\frac{l_{\mathrm{ref}}^{k_{\mathrm{sc}}} \left(k_{\mathrm{sc}} \, 10^4 + \alpha \, u \ln 10\right)}{10^{[4 + \alpha(u - l_{\mathrm{ref}})10^{-4}]} u^{k_{\mathrm{sc}} + 1}}.
$$

Combining the previous expressions, we get

$$
\begin{aligned}
\frac{\partial \ln p(d_k[n] | \mathcal{H}_1; \boldsymbol{\theta})}{\partial \boldsymbol{\theta}} &= \frac{d_k[n] - P_{D,k}}{P_{D,k}(1 - P_{D,k})} \\
&\quad \times p_{\mathcal{N}(0,1)}\left(\sqrt{\frac{\tau_k}{\sigma_\xi^2 g^2(u) + \sigma_w^2}}\right) \\
&\quad \times \frac{\psi(u) \sigma_\xi^2 \sqrt{\tau_k}}{u \left[\sigma_\xi^2 g^2(u) + \sigma_w^2\right]^{3/2}} (\boldsymbol{\theta} - \boldsymbol{s}_k),
\end{aligned}
$$

and then

$$
\boldsymbol{I}_k(\boldsymbol{\theta}) = \frac{p_{\mathcal{N}(0,1)}^2 \left(\sqrt{\frac{\tau_k}{\sigma_\xi^2 g^2(u) + \sigma_w^2}}\right)}{P_{D,k}^2 (1 - P_{D,k})^2} \frac{\psi^2(u) \sigma_\xi^4 \tau_k}{u^2 \left[\sigma_\xi^2 g^2(u) + \sigma_w^2\right]^3} \times (\boldsymbol{\theta} - \boldsymbol{s}_k)(\boldsymbol{\theta} - \boldsymbol{s}_k)^T, \tag{40}
$$

where the expectation has been calculated with the knowledge that $d_k[n] | \mathcal{H}_1 \sim \mathcal{B}(P_{D,k})$. Finally, replacing Eq. (40) into Eq. (39), we get the CRLB via Eq. (38).

REFERENCES

[1] H. Fang and M. Duan, *Offshore Operation Facilities: Equipment and Procedures*. Amsterdam, The Netherlands: Elsevier, 2014.

[2] Y. Bai and Q. Bai, *Subsea Engineering Handbook*. Houston, TX, USA: Elsevier, 2012.

[3] F. Pallavicini, "Developement of offshore fields," in *Encyclopaedia of Hydrocarbons—Exploration, Production and Transport*, vol. 1. Rome, Italy: Treccani, 2005, ch. 5.2, pp. 609–628.

[4] C. Mai, S. Pedersen, L. Hansen, K. L. Jepsen, and Z. Yang, "Subsea infrastructure inspection: A review study," in *Proc. IEEE Int. Conf. Underwater Syst. Technol., Theory Appl. (USYS)*, Penang, Malaysia, Dec. 2016, pp. 71–76.

[5] N. Paltrinieri, F. Khan, P. Amyotte, and V. Cozzani, "Dynamic approach to risk management: Application to the Hoeganaes metal dust accidents," *Process Saf. Environ. Protection*, vol. 92, no. 6, pp. 669–679, Nov. 2014.

[6] V. Villa, N. Paltrinieri, F. Khan, and V. Cozzani, "Towards dynamic risk analysis: A review of the risk assessment approach and its limitations in the chemical process industry," *Saf. Sci.*, vol. 89, pp. 77–93, Nov. 2016.

[7] T. Grøtan and N. Paltrinieri, "Dynamic risk management in the perspective of a resilient system," in *Dynamic Risk Analysis in the Chemical and Petroleum Industry*. Amsterdam, The Netherlands: Elsevier, 2016, pp. 245–257.

[8] N. Paltrinieri, L. Comfort, and G. Reniers, "Learning about risk: Machine learning for risk assessment," *Saf. Sci.*, vol. 118, pp. 475–486, Oct. 2019.

[9] M. A. Adegboye, W.-K. Fung, and A. Karnik, "Recent advances in pipeline monitoring and oil leakage detection technologies: Principles and approaches," *Sensors*, vol. 19, no. 11, p. 2548, Jun. 2019.

[10] U. Baroudi, A. A. Al-Roubaiey, and A. Devendiran, "Pipeline leak detection systems and data fusion: A survey," *IEEE Access*, vol. 7, pp. 97426–97439, 2019.

[11] *Recommended Practice RP-F302 Offshore Leak Detection*, DNV-GL, Oslo, Norway, Apr. 2016.

[12] H. V. Fuchs and R. Riehle, "Ten years of experience with leak detection by acoustic signal analysis," *Appl. Acoust.*, vol. 33, no. 1, pp. 1–19, 1991.

[13] E. G. Eckert, J. W. Maresca, R. W. Hillger, and J. J. Yezzi, "Location of leaks in pressurized petroleum pipelines by means of passive-acoustic sensing methods," in *Leak Detection for Underground Storage Tanks*, P. Durgin and T. Young, Eds. West Conshohocken, PA, USA: ASTM International, 1993, pp. 53–69.

[14] J. Li, C. Wang, Q. Zheng, and Z. Qian, "Leakage localization for long distance pipeline based on compressive sensing," *IEEE Sensors J.*, vol. 19, no. 16, pp. 6795–6801, Aug. 2019.

[15] M. Meribout, "A wireless sensor network-based infrastructure for real-time and online pipeline inspection," *IEEE Sensors J.*, vol. 11, no. 11, pp. 2966–2972, Nov. 2011.

[16] T. R. Sheltami, A. Bala, and E. M. Shakshuki, "Wireless sensor networks for leak detection in pipelines: A survey," *J. Ambient Intell. Humanized Comput.*, vol. 7, no. 3, pp. 347–356, Jun. 2016.

[17] N. Paltrinieri, G. Landucci, and P. Salvo Rossi, "An integrated approach to support the dynamic risk assessment of complex industrial accidents," *Chem. Eng. Trans.*, vol. 77, pp. 265–270, Sep. 2019.

[18] M. Bucelli, I. B. Utne, P. Salvo Rossi, and N. Paltrinieri, "A system engineering approach to subsea spill risk management," *Saf. Sci.*, vol. 123, Mar. 2020, Art. no. 104560.

[19] M. R. Akhondi, A. Talevski, S. Carlsen, and S. Petersen, "Applications of wireless sensor networks in the oil, gas and resources industries," in *Proc. 24th IEEE Int. Conf. Adv. Inf. Netw. Appl.*, Perth, WA, Australia, Apr. 2010, pp. 941–948.

[20] P. K. Varshney, *Distributed Detection and Data Fusion*. New York, NY, USA: Springer-Verlag, 1997.

[21] A. Shoari, G. Mateos, and A. Seyedi, "Analysis of target localization with ideal binary detectors via likelihood function smoothing," *IEEE Signal Process. Lett.*, vol. 23, no. 5, pp. 737–741, May 2016.

[22] Z. Chair and P. K. Varshney, "Optimal data fusion in multiple sensor detection systems," *IEEE Trans. Aerosp. Electron. Syst.*, vol. AES-22, no. 1, pp. 98–101, Jan. 1986.

[23] R. Niu, P. K. Varshney, and Q. Cheng, "Distributed detection in a large wireless sensor network," *Inf. Fusion*, vol. 7, no. 4, pp. 380–394, Dec. 2006.

[24] B. Chen, R. Jiang, T. Kasetkasem, and P. K. Varshney, "Channel aware decision fusion in wireless sensor networks," *IEEE Trans. Signal Process.*, vol. 52, no. 12, pp. 3454–3458, Dec. 2004.

[25] X. Wang, G. Li, and P. K. Varshney, "Distributed detection of weak signals from one-bit measurements under observation model uncertainties," *IEEE Signal Process. Lett.*, vol. 26, no. 3, pp. 415–419, Mar. 2019.

[26] D. Ciuonzo, G. Papa, G. Romano, P. Salvo Rossi, and P. Willett, "One-bit decentralized detection with a Rao test for multisensor fusion," *IEEE Signal Process. Lett.*, vol. 20, no. 9, pp. 861–864, Sep. 2013.

[27] D. Ciuonzo, P. Salvo Rossi, and P. Willett, "Generalized Rao test for decentralized detection of an uncooperative target," *IEEE Signal Process. Lett.*, vol. 24, no. 5, pp. 678–682, May 2017.

[28] D. Ciuonzo and P. Salvo Rossi, "Distributed detection of a non-cooperative target via generalized locally-optimum approaches," *Inf. Fusion*, vol. 36, pp. 261–274, Jul. 2017.

[29] D. Ciuonzo, G. Romano, and P. Salvo Rossi, "Channel-aware decision fusion in distributed MIMO wireless sensor networks: Decode-and-fuse vs. decode-then-fuse," *IEEE Trans. Wireless Commun.*, vol. 11, no. 8, pp. 2976–2985, Aug. 2012.

[30] P. Salvo Rossi, D. Ciuonzo, T. Ekman, and H. Dong, "Energy detection for MIMO decision fusion in underwater sensor networks," *IEEE Sensors J.*, vol. 15, no. 3, pp. 1630–1640, Mar. 2015.

[31] P. Salvo Rossi, D. Ciuonzo, K. Kansanen, and T. Ekman, "Performance analysis of energy detection for MIMO decision fusion in wireless sensor networks over arbitrary fading channels," *IEEE Trans. Wireless Commun.*, vol. 15, no. 11, pp. 7794–7806, Nov. 2016.

[32] A. Shoari and A. Seyedi, "Localization of an uncooperative target with binary observations," in *Proc. IEEE 11th Int. Workshop Signal Process. Adv. Wireless Commun. (SPAWC)*, Marrakech, Morocco, Jun. 2010, pp. 1–5.

[33] J. Zhao, Q. Zhao, Z. Li, and Y. Liu, "An improved weighted centroid localization algorithm based on difference of estimated distances for wireless sensor networks," *Telecommun. Syst.*, vol. 53, no. 1, pp. 25–31, May 2013.

[34] Q. Dong and X. Xu, "A novel weighted centroid localization algorithm based on RSSI for an outdoor environment," *J. Commun.*, vol. 9, no. 3, pp. 279–285, 2014.

[35] S. Durocher and D. Kirkpatrick, "The Steiner centre of a set of points: Stability, eccentricity, and applications to mobile facility location," *Int. J. Comput. Geometry Appl.*, vol. 16, no. 4, pp. 345–371, Aug. 2006.

[36] Q. Zhou, X. Li, and Y. Xu, "Smallest enclosing circle based localization approach for wireless sensor networks," in *Proc. WRI Int. Conf. Commun. Mobile Comput.*, Kunming, China, Jan. 2009, pp. 61–65.

[37] A. Vempaty, H. He, B. Chen, and P. K. Varshney, "On quantizer design for distributed Bayesian estimation in sensor networks," *IEEE Trans. Signal Process.*, vol. 62, no. 20, pp. 5359–5369, Oct. 2014.

[38] A. Kose and E. Masazade, "A multiobjective optimization approach for adaptive binary quantizer design for target tracking in wireless sensor networks," in *Proc. IEEE Int. Conf. Multisensor Fusion Integr. Intell. Syst. (MFI)*, San Diego, CA, USA, Sep. 2015, pp. 31–36.

[39] D. Ciuonzo and P. Salvo Rossi, "Quantizer design for generalized locally optimum detectors in wireless sensor networks," *IEEE Wireless Commun. Lett.*, vol. 7, no. 2, pp. 162–165, Apr. 2018.

[40] J. Fang, Y. Liu, H. Li, and S. Li, "One-bit quantizer design for multisensor GLRT fusion," *IEEE Signal Process. Lett.*, vol. 20, no. 3, pp. 257–260, Mar. 2013.

[41] S. Kar, H. Chen, and P. K. Varshney, "Optimal identical binary quantizer design for distributed estimation," *IEEE Trans. Signal Process.*, vol. 60, no. 7, pp. 3896–3901, Jul. 2012.

[42] G. Tabella, N. Paltrinieri, V. Cozzani, and P. Salvo Rossi, "Data fusion for subsea oil spill detection through wireless sensor networks," in *Proc. IEEE Sensors*, Rotterdam, The Netherlands, Oct. 2020, pp. 1–4.

[43] G. Tabella, N. Paltrinieri, V. Cozzani, and P. Salvo Rossi, "Subsea oil spill risk management based on sensor networks," *Chem. Eng. Trans.*, vol. 82, pp. 199–204, Oct. 2020.

[44] W. H. Thorp, "Analytic description of the low-frequency attenuation coefficient," *J. Acoust. Soc. Amer.*, vol. 42, no. 1, p. 270, 1967.

[45] M. Schulkin and H. W. Marsh, "Sound absorption in sea water," *J. Acoust. Soc. Amer.*, vol. 34, no. 6, pp. 864–865, 1962.

[46] F. H. Fisher and V. P. Simmons, "Sound absorption in sea water," *J. Acoust. Soc. Amer.*, vol. 62, no. 3, pp. 558–564, 1977.

[47] M. A. Ainslie and J. G. McColm, "A simplified formula for viscous and chemical absorption in sea water," *J. Acoust. Soc. Amer.*, vol. 103, no. 3, pp. 1671–1672, Mar. 1998.

[48] R. E. Francois and G. R. Garrison, "Sound absorption based on ocean measurements: Part I: Pure water and magnesium sulfate contributions," *J. Acoust. Soc. Amer.*, vol. 72, no. 3, pp. 896–907, Sep. 1982.

[49] R. E. Francois and G. R. Garrison, "Sound absorption based on ocean measurements. Part II: Boric acid contribution and equation for total absorption," *J. Acoust. Soc. Amer.*, vol. 72, no. 6, pp. 1879–1890, Dec. 1982.

[50] P. C. Etter, *Underwater Acoustic Modeling and Simulation*, 5th ed. Boca Raton, FL, USA: CRC Press, 2018.

[51] H. Medwin, "Speed of sound in water: A simple equation for realistic parameters," *J. Acoust. Soc. Amer.*, vol. 58, no. 6, pp. 1318–1319, Dec. 1975.

[52] K. V. Mackenzie, "Nine-term equation for sound speed in the oceans," *J. Acoust. Soc. Amer.*, vol. 70, no. 3, pp. 807–812, Sep. 1981.

[53] V. A. Del Grosso, "New equation for the speed of sound in natural waters (with comparisons to other equations)," *J. Acoust. Soc. Amer.*, vol. 56, no. 4, pp. 1084–1091, Oct. 1974.

[54] C. Chen and F. J. Millero, "Speed of sound in seawater at high pressures," *J. Acoust. Soc. Amer.*, vol. 62, no. 5, pp. 1129–1135, Nov. 1977.

[55] F. J. Millero and X. Li, "Comments 'on on equations for the speed of sound in seawater' [J. Acoust. Soc. Am. 93, 255–275 (1993)]," *J. Acoust. Soc. Amer.*, vol. 95, no. 5, pp. 2757–2759, 1994.

[56] G. S. K. Wong and S. Zhu, "Speed of sound in seawater as a function of salinity, temperature, and pressure," *J. Acoust. Soc. Amer.*, vol. 97, no. 3, pp. 1732–1736, Mar. 1995.

[57] S. Kay, *Fundamentals of Statistical Signal Processing: Detection Theory* (Prentice-Hall Signal Processing Series), 1st ed. Upper Saddle River, NJ, USA: Prentice-Hall, 1998.

[58] W. J. Youden, "Index for rating diagnostic tests," *Cancer*, vol. 3, no. 1, pp. 32–35, 1950.

[59] H. V. Poor and O. Hadjiliadis, *Quickest Detection*. Cambridge, U.K.: Cambridge Univ. Press, 2008.

[60] E. Bjørnbom. (2011). *Goliat–Leak Detection and Monitoring From Template to Satellite*. Accessed: Dec. 29, 2020. [Online]. Available: https://www.norskoljeoggass.no/globalassets/dokumenter/drift/presentasjonerarrangementer/subsea-leak-detection–2011/4.-enino_n1862090_v1_eni_presentation_-_olf_seminar_-_subsea_leak_detection_-_03_november_2011.pdf

[61] E. Røsby. (2011). *Goliat Development Project—Subsea Leak Detection Design*. Accessed: Dec. 29, 2020. [Online]. Available: https://www.norskoljeoggass.no/globalassets/dokumenter/drift/presentasjonerarrangementer/subsea-leak-detection–2011/15.-goliat-development-project_subsea_leak_detection_3_nov_2011_elling-rosby.pdf

[62] *OREDA Offshore Reliability Data Handbook*, 4th ed., SINTEF, OREDA Participants, Bhubaneswar, India, 2002.

[63] Institute of Marine Research. (Sep. 9, 2020). *Mareano*. [Online]. Available: http://www.mareano.no/kart

[64] A. A. Vetrov and E. A. Romankevich, *Carbon Cycle in the Russian Arctic Seas*. Berlin, Germany: Springer, 2004.

[65] M. Stojanovic, "On the relationship between capacity and distance in an underwater acoustic communication channel," in *Proc. 1st ACM Int. Workshop Underwater Netw. (WUWNet)*, Oct. 2006, pp. 34–43.

Nicola Paltrinieri received the B.Sc. degree in chemical engineering, the M.Sc. degree (*summa cum laude*) in chemical and process engineering, and the Ph.D. degree in environmental, safety and chemical engineering from the University of Bologna, Italy, in 2005, 2008, and 2012, respectively. From 2012 to 2016, he was a Research Scientist with the Department of Safety Research, SINTEF Technology and Society, Norway. In 2012, he held a postdoctoral position with the University of Bologna. He has been an Associate Professor of Risk Analysis with the Norwegian University of Science and Technology (NTNU), Norway, and an Adjunct Professor in Offshore HSE Management with the University of Bologna, Italy, since 2016. His research interests include both the method and the application of risk analysis within socio-technical systems. Regarding the former, he has investigated the concepts and techniques supporting dynamic risk analysis, from uncertainty to machine learning. Regarding the latter, he has worked on risk analysis for safety-critical emerging technologies, such as hydrogen technologies. He is a Chartered Engineer at the British Engineering Council Register and a Charted Scientist at the British Science Council Register. He is a member of the editorial boards of the *Journal of Marine Science and Engineering*, *Journal of Risk Research* and *Safety in Extreme Environments*, the Board of the NTNU Team Hydrogen, and the Board and Treasurer of the Society of Risk Analysis—Europe. He also serves as a member for the scientific committees for the ESREL, Loss Prevention and CISAP conferences, since 2016. He serves as Norwegian delegate for the Working Party on Loss Prevention and Safety Promotion within the European Federation of Chemical Engineering. He is a Co-Chair on Accident and Incident modeling, and the European Safety and Reliability Association Technical Committee. He serves as an Associate Editor for the journal *Safety Science*.

Gianluca Tabella (Graduate Student Member, IEEE) was born in Suzzara, Italy, in 1993. He received the B.Sc. degree in chemical and biochemical engineering (with specialization in process engineering) and the M.Sc. degree in chemical and process engineering (with specialization in offshore engineering) from the University of Bologna, Italy, in 2017 and 2019, respectively. He is currently pursuing the Ph.D. degree in electronics and telecommunications with the Department of Electronic Systems, Norwegian University of Science and Technology (NTNU), Norway, within the Signal Processing Research Group. He carried out his master's thesis with the Department of Mechanical and Industrial Engineering, NTNU.

His research interests include distributed detection and localization for safety and risk analysis with a focus on industrial and Oil and Gas applications.

Valerio Cozzani received the M.Sc. degree (*cum laude*) and the Ph.D. degree in chemical engineering from the University of Pisa, Italy, in 1992 and 1997, respectively. From 1995 to 1996, he was a Visiting Scientist with the Industrial Hazards Unit, European Community Joint Research Centre, Institute for Safety, Informatics and Systems. From 1997 to 1998, he was a Research Assistant with the National Research Group on Chemical and Environmental Risk of the Italian National Research Council (CNR). From 1995 to 1996, he was a Visiting Scientist with the Industrial Hazards Unit, European Community Joint Research Centre, Institute for Safety, Informatics and Systems. From 1998 to 2002, he was a Lecturer with the Faculty of Engineering and a member of the Department of Chemical Engineering, University of Pisa, Italy. From 2002 to 2006, he was an Associate Professor with the Faculty of Engineering and a member of the Department of Chemical Engineering, University of Bologna, Italy. Since 2006, he has been a Professor with the School of Engineering and a member of the Department of Civil, Chemical, Environmental and Materials Engineering, University of Bologna, Italy. At the University of Bologna, he is the Director of the M.Sc. in offshore engineering, leads the Laboratory of Industrial Safety and Environmental Sustainability, associated to the IChemE Safety Centre, and coordinates several courses for professionals in the fields of industrial safety and design of Oil and Gas facilities. His specific research topics, such as the assessment of major accidents involving dangerous substances caused by external hazard factors, cascading events and domino effects; the safety and sustainability assessment of innovative chemical processes; the safety assessment of alternative fuel systems, and synthetic fuel supply chains. He chairs the ESRA Technical Committee on Chemical and Process Industry. He is the Italian Delegate at the EFCE Working Party on Loss Prevention in the Process Industry. He serves as an Associate Editor for *Safety Science* and a member of the Editorial Board for Elsevier publications on chemical engineering, for the *Journal of Hazardous Materials* and the *Journal of Loss Prevention in the Process Industry*. He also serves as a member for the scientific committees of ESREL conferences since 2008, and chairs the scientific committee of CISAP conferences since 2012.

Pierluigi Salvo Rossi (Senior Member, IEEE) was born in Naples, Italy, in 1977. He received the Dr.Eng. degree (*summa cum laude*) in telecommunications engineering and the Ph.D. degree in computer engineering from the University of Naples "Federico II", Italy, in 2002 and 2005, respectively. He held visiting appointments with the Department of Electrical and Computer Engineering, Drexel University, Philadelphia, PA, USA, the Department of Electrical and Information Technology, Lund University, Sweden, the Department of Electronics and Telecommunications, Norwegian University of Science and Technology (NTNU), Norway, and the Excellence Center for Wireless Sensor Networks, Uppsala University, Sweden. From 2005 to 2008, he held postdoctoral positions with the Department of Computer Science and Systems, University of Naples "Federico II," Italy, the Department of Information Engineering, Second University of Naples, Italy, and the Department of Electronics and Telecommunications, NTNU, Norway. From 2008 to 2014, he was an Assistant Professor (tenured in 2011) in telecommunications with the Department of Industrial and Information Engineering, Second University of Naples, Italy.

From 2014 to 2016, he was an Associate Professor in signal processing with the Department of Electronics and Telecommunications, NTNU, Norway. From 2016 to 2017, he was a Full Professor in signal processing with the Department of Electronic Systems, NTNU, Norway. From 2017 to 2019, he was a Principal Engineer with the Department of Advanced Analytics and Machine Learning, Kongsberg Digital AS, Norway. Since 2019, he has been a Full Professor of Statistical Machine Learning with the Department of Electronic Systems, NTNU, Norway, and also the Director of IoT@NTNU. Since 2021, he is also a (part-time) Research Scientist with the Department of Gas Technology, SINTEF Energy Research, Norway. His research interests include communication theory, data fusion, machine learning, and signal processing. He serves as an Executive Editor for the IEEE COMMUNICATIONS LETTERS since 2019, an Area Editor for the IEEE OPEN JOURNAL OF THE COMMUNICATIONS SOCIETY since 2019, an Associate Editor for the IEEE TRANSACTIONS ON SIGNAL AND INFORMATION PROCESSING OVER NETWORKS since 2019, and the IEEE SENSORS JOURNAL since 2021. He was an Associate Editor of the IEEE TRANSACTIONS ON WIRELESS COMMUNICATIONS from 2015 to 2020, a Senior Editor from 2016 to 2019 and an Associate Editor from 2012 to 2016 of the IEEE COMMUNICATIONS LETTERS. He was awarded as an Exemplary Senior Editor of the IEEE COMMUNICATIONS LETTERS in 2018.